Available online at www.sciencedirect.com
ScienceDirect
Energy Reports 9 (2023) 647–655
www.elsevier.com/locate/egyr

2022 The 3rd International Conference on Power and Electrical Engineering (ICPEE 2022)
29–31 December, Singapore

Design of a robust and practicable SSI damping controller using H$^\infty$ technique for series compensated DFIG-based wind farms

Mohsen Ghafouri[a], Ulas Karaagac[b,*], Jean Mahseredjian[c], Ilhan Kocar[b], Meng Lei[b]

[a] *Concordia Institute for Information Systems Engineering, Concordia University, Montreal, QC, Canada*
[b] *Department of Electrical Engineering, The Hong Kong Polytechnic University, Hung Hom, Kowloon, Hong Kong*
[c] *Department of Electrical Engineering, Polytechnique Montréal, Montreal, QC, Canada*

Received 20 April 2023; accepted 19 May 2023
Available online 1 June 2023

Abstract

This paper designs a robust and practicable subsynchronous interaction (SSI) damping controller using H$^\infty$ technique for the safe operation of series capacitor compensated wind farms (WFs) with doubly-fed induction generator (DFIG) wind turbines (WTs). Mixed sensitivity control design together with pole placement are formulated into a set of linear matrix inequalities (LMIs) to obtain the controller parameters. The LMI technique allows to include both desirable frequency and time domain specifications. The proposed damping controller is integrated into the WT controller (WTC) and receives the DFIG converter currents as inputs. The implementation of the proposed controller does not require any communication links between the WTs and WF secondary control layer. The controller output signals are applied to the inner control loops of DFIG converters and are dynamically limited for the desired fault-ride-through (FRT) performance. The effectiveness of the damping controller is verified through detailed electromagnetic transient (EMT) simulations. In these simulations, the complete medium-voltage (MV) collector grid is modeled with all details, and it is assumed that the wind speed at the location of each turbine follows a Gaussian distribution. The collected results confirm the accuracy of the modeling of the entire WF as an aggregated WT with the average wind speed.

Peer-review under responsibility of the scientific committee of the 3rd International Conference on Power and Electrical Engineering.

Keywords: Doubly-fed induction generator (DFIG); H$^\infty$ control; Linear matrix inequality (LMI); Pole placement; Series capacitor compensation; Subsynchronous interaction (SSI); Wind farm

1. Introduction

Doubly-fed induction generator (DFIG)-based wind farms (WFs) can adversely interact with the series compensated AC grids at subsynchronous frequency range [1]. This phenomenon is called subsynchronous interaction (SSI) and confirmed with several real-life incidents [2]. Several studies have been conducted for SSI mitigation particularly

* Corresponding author.
E-mail address: ulas.karaagac@polyu.edu.hk (U. Karaagac).

https://doi.org/10.1016/j.egyr.2023.05.094

Peer-review under responsibility of the scientific committee of the 3rd International Conference on Power and Electrical Engineering.

using SSI damping controllers (SSDC) [3–14] due to their low investment costs. These controllers are often designed to operate in the secondary control level of the WF (i.e. central implementation like WF controller (WFC)) as the entire system inside the WF is represented with a single aggregated wind turbine (WT). On the other hand, the central implementation of SSDC may result in several practical issues such as vulnerability to delays in the feedback control loops [12,13]. Especially, malfunction of sensors, or cyber-attacks on the communication structure between the WTs and central SSDC can result in latency in the feedback loops and compromise the system stability [14]. On the other hand, integrating SSDC into the WT controller (WTC) may not provide the desired damping in all operating conditions (such as WT outage scenarios) unless a robust or adaptive control approach is adopted.

The robust control techniques such as H^{∞} mixed-sensitivity and μ-technique have been used in various power system applications [15–19]. The main advantages of such robust techniques over the other existing design methods have been detailed in [20]. The H^{∞} and μ-based techniques are well-known frequency domain-based robust control methods that can improve the damping of the closed-loop system despite uncertainties in system parameters. The linear matrix inequality (LMI) framework allows mixing the objectives in time and frequency domains [15,21]. Confining the closed-loop system poles into a pre-desired region of the s-plane and H^{∞} design of the controller can be merged into a set of LMIs, and solved simultaneously. The use of a numerical approach for solving the control problem through the LMI formulation is advantageous as the resulting controller does not suffer from pole-zero cancellation issues as discussed in [21].

This paper proposes using a robust mixed-sensitivity H^{∞} control with regional pole placement for SSDC design to provide robustness and the desired performance characteristics, e.g., reference tracking and disturbance rejection. In addition, using the pole placement technique confines the closed-loop poles within the desired region where the SSI modes are perfectly damped. The proposed SSDC is integrated into the WTC and it only receives the DFIG converter currents as its inputs. Hence, its implementation does not require any communication links between the WTs and WF secondary control layer. The SSDC output signals are added to the inner current control loops of the DFIG converters and they are dynamically limited to achieve the desired DFIG transient response against voltage sags and swells.

SSDC is designed using the simple linearized version of the system. However, its effectiveness is verified through detailed electromagnetic transient (EMT) simulations. In simulation model, WF includes the complete medium voltage (MV) collector grid model with all details. Different wind speeds are applied to each WT considering a reasonable Gaussian distribution. Representative simulations are also performed with the aggregated model to test its precision.

The paper is organized as follows. Section 2 presents the system under study. The mixed-sensitivity technique and SSDC design are presented in Sections 3 and 4, respectively. Section 5 presents the EMT simulation results. Section 6 concludes the paper.

2. System under study

The 500 kV test system [12] is shown in Fig. 1(a). The WF consists of 268 DFIG WTs each with the rating of 1.5 MW. Line-1 and Line-2 connects the WF to two strong systems System-1 and System-2, respectively. Line-1 is 50% series capacitor compensated line. Disconnection of Line-2 leaves the WF radially connected to the series capacitor compensated line.

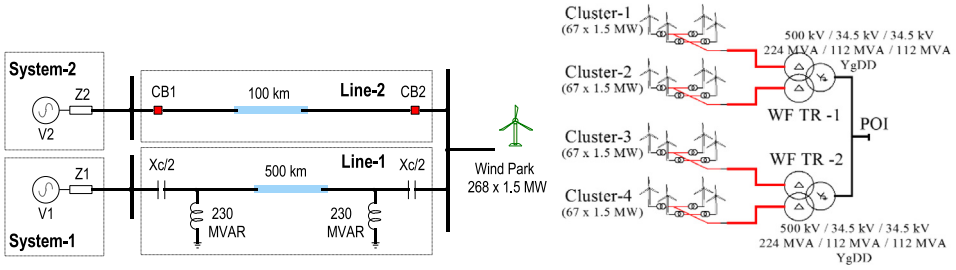

(a) 500 kV test system

(b) Single line diagram of the considered wind farm

Fig. 1. The system under study.

As shown in Fig. 1(b), the WF is divided into four clusters and connected to the transmission grid through two WF transformers. All clusters are assumed to be identical, and each contains 67 WTs on five 34.5 kV feeders. The WF cluster is inspired from an actual system. Reader should refer to [12] for details.

As seen in Fig. 2(a), the WF reactive power generation has marginal impact on SSI mode damping. On the other hand, the equivalent rotor resistance of DFIG decreases at subsynchronous frequency with the decrease in wind speed. Hence, the decrease in wind speed also causes significant decrease in the SSI mode damping. From Fig. 2, it can be concluded that the most severe SSI problem can be expected at the slowest permissible wind speed ($V = 0.6$ pu) when there are around 150 WTs in service.

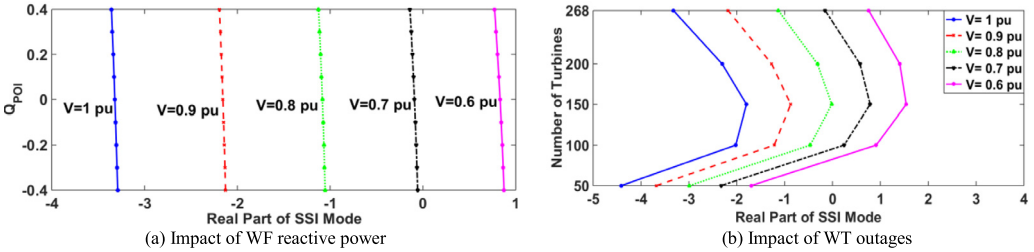

(a) Impact of WF reactive power (b) Impact of WT outages

Fig. 2. Impact of WF reactive power and WT outages on damping at different wind speeds.

Details of the linearized model can be found in [10]. The simplifications in the linearized model enables straightforward analysis and low-order controller design. However, the obtained results remain conservative due to disregarding the phase locking loop (PLL) dynamics and especially the low-pass measuring filters [22].

3. Mixed-sensitivity control design

The state-space representation of the WF-integrated power system can be expressed as:

$$\begin{aligned} \dot{\mathbf{x}} &= \mathbf{Ax} + \mathbf{Bu} \\ \mathbf{y} &= \mathbf{Cx} + \mathbf{Du} \end{aligned} \tag{1}$$

In this equation, **x**, **u,** and **y** are, respectively, the system state, input and output vectors. Moreover, the linearized behavior of the system is presented by matrices **A**, **B**, **C,** and **D.**

Fig. 3(a) depicts the schematic used for controller design based on standard mixed-sensitivity technique. In this schematic, the open loop system is modeled by its transfer function G(s). This transfer function is obtained from the state-space linear representation of the under-study system, i.e., A, B, C, and D, as expressed in Eq. (1). **K(s)** depicts the transfer function of the envisioned controller. Moreover, the transfer function between disturbance (**d**) and output (**y**) can be written as $\mathbf{S} = (\mathbf{I} - \mathbf{GK})^{-1}$. Therefore, minimization of $\|\mathbf{S}\|_\infty$ will result in a controller design, which can effectively reject the disturbances. Additionally, the transfer function between the disturbance and controller input, i.e., $\|\mathbf{KS}\|_\infty$, should be minimized. However, it is not possible to design a controller that can minimize both **S** and **KS** in a frequency range. Thus, for each transfer function, a frequency range is defined, and the value of the functions are minimized in their respective range. To do so, two weighting filters $\mathbf{W_1}$ and $\mathbf{W_2}$ are defined to minimize each transfer function over a pre-specified frequency range. In this scheme, $\mathbf{W_1}$ is a low-pass filter that aims to reject the disturbances in a low frequency range, whereas $\mathbf{W_2}$ is a high-pass filter, which is designed to decrease the controller's effort in high-frequency ranges.

Based on these discussions, the design problem will be a **(S/KS)** mixed-sensitivity, which can be expressed as:

$$\min_{\mathbf{K}\in\Omega} \left\| \begin{matrix} \mathbf{W_1}(s)\mathbf{S}(s) \\ \mathbf{W_2}(s)\mathbf{K}(s)\mathbf{S}(s) \end{matrix} \right\|_\infty < \gamma \tag{2}$$

In this equation, Ω represents the set of all the transfer functions that are able to stabilize the plant, and γ is a number that represents the robustness level of the system. It should be noted that a small value of γ results in a more robust controller, whereas large value of γ results in a system with low stability margins. To solve this equation,

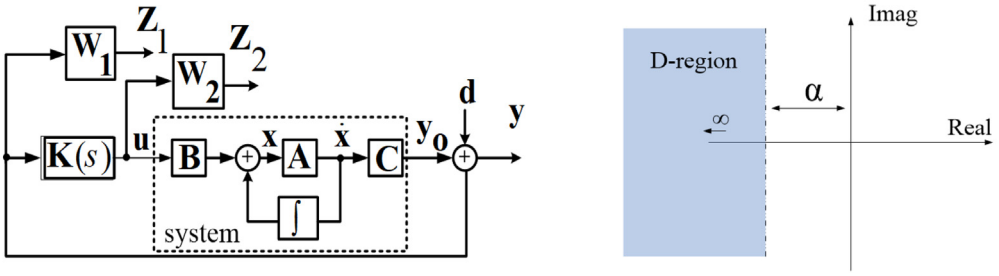

(a) Controller design scheme (b) Pole placement desired region

Fig. 3. The controller design scheme and pole placement desired region.

the term inside the infinity norm, i.e., the transfer function between d and z, should be expressed by closed-loop matrices as:

$$\mathbf{T_{zd}}(s) = \begin{bmatrix} \mathbf{W_1}(s)\mathbf{S}(s) \\ \mathbf{W_2}(s)\mathbf{K}(s)\mathbf{S}(s) \end{bmatrix} = \mathbf{C_{cl}}(s\mathbf{I} - \mathbf{A_{cl}})^{-1}\mathbf{B_{cl}} + \mathbf{D_{cl}} \tag{3}$$

The matrices of the state-space representation of the closed-loop system can be found in [16].

For robustness, $\|\mathbf{T_{zd}}\|_\infty < \gamma$. Then, for partitioned matrices, such as the ones discussed above, the bounded real lemma and Schur's formula [23] state that a closed-loop system will be asymptotically stable if the LMI of (4) holds:

$$\begin{bmatrix} \mathbf{A_{cl}}^T\mathbf{X} + \mathbf{X}\mathbf{A_{cl}} & \mathbf{B_{cl}} & \mathbf{X}\mathbf{C_{cl}}^T \\ \mathbf{B_{cl}}^T & -\gamma\mathbf{I} & \mathbf{D_{cl}}^T \\ \mathbf{C_{cl}}\mathbf{X} & \mathbf{D_{cl}} & -\gamma\mathbf{I} \end{bmatrix} < \mathbf{0} \tag{4}$$

where

$$\mathbf{X} = \mathbf{X^T} > \mathbf{0} \tag{5}$$

For the proposed controller, it is a requirement to stabilize the system and damp the oscillations within a specified settling time. This is achievable if all the eigenvalues of the closed-loop system lie in an appropriate area of the s-plane. Assuming the pole placement region to be shifted half plane, the following LMI holds [24]:

$$\mathbf{A}^T\mathbf{P_{LMI}} + \mathbf{A}\mathbf{P_{LMI}} - \mathbf{C}^T\mathbf{W} - \mathbf{W}^T\mathbf{C} + 2\alpha\mathbf{P_{LMI}} < 0 \tag{6}$$

where $\mathbf{P_{LMI}}$ is a positive definite matrix, and α is the maximum acceptable value for the real part of closed-loop system eigenvalues (see Fig. 3(b)).

Based on these equations, the controller can be designed using the LMIs if the solvers are able to find two positive semi-definite matrices $\mathbf{P_{LMI}} = \mathbf{X}$ and $\mathbf{K}$ that satisfy (4) and (5) simultaneously. It should be noted that $\mathbf{K}$ can be retrieved from the closed-loop matrices, which are expressed in (3), by solving LMIs (4) and (5). The weighting filters can also be used to achieve a multi-objective design. A set of guidelines for proper design of these weighting filters can be found in [24]. To solve the LMIs, the *Robust Toolbox* of MATLAB software has been used. Since the order of the controller, which is designed using this technique, is typically high, a model order reduction technique is required. It should be noted that due to sensitivity to noise and implementation difficulties, in most practical cases, it is not feasible or preferable to use high-order controllers. Thus, in this work, a model reduction technique based on the Hankel singular value (HSV) is utilized. The HSV of a state-space system defines the energy in each of its states [25]. The system model reduction based on keeping the highest energy states preserves most of its characteristics. The HSV defines as:

$$\sigma_h^i = \sqrt{\lambda_i(\mathbf{MN})} \tag{7}$$

In this equation, matrices $\mathbf{N}$ and $\mathbf{M}$ represent the controllability and observability grammians satisfying these equations:

$$\mathbf{A}\mathbf{M} + \mathbf{M}\mathbf{A}^T + \mathbf{B}\mathbf{B}^T = \mathbf{0} \tag{8}$$

$$\mathbf{A}^T\mathbf{N} + \mathbf{N}\mathbf{A} + \mathbf{C}^T\mathbf{C} = \mathbf{0} \tag{9}$$

The Hankel norm of a system is defined to be its largest HSV. Based on the Hankel norm of a system, this technique finds a reduced order model of a system in a way that $\|\mathbf{G_{nom}} - \mathbf{G_{red}}\|_\infty$, i.e., the infinity norm of error, becomes minimized.

4. SSI damping controller (SSDC) design

SSDC design is performed based on H^∞ mixed-sensitivity method combined with the pole placement technique. To avoid communication requirement between the WTs and WF secondary control layer, only the rotor side converter (RSC) and grid side converter (GSC) output currents are selected as the damping controller input signals.

$$\mathbf{y} = [i_{qr}\, i_{dr}\, i_{qg}\, i_{dg}]^T \tag{10}$$

where i_{dr} and i_{qr} are the dq reference frame RSC currents, and i_{dg} and i_{qg} are the dq reference frame GSC currents.

The outputs of SSDC are added to the inner loop current references of both RSC and GSC. These assumptions address a simplified system with 34 states, 4 inputs and 4 outputs. Similar to [10–14], the desired FRT operation is achieved by limiting the outputs of SSDC dynamically.

The pole placement technique moves all the system modes to a specified region. However, shifting certain modes (especially the mechanical modes) far to the left side of the s-plane needs high control signals. This may cause converter saturation, hence, reduced performance in SSDC. Therefore, the order of the system is decreased by Hankel reduction order techniques using *Robust Control Toolbox* [26] of the *MATLAB* software to consider mainly the SSI modes.

From the open-loop system HSVs, shown Fig. 4, the SSI modes are unstable. It can be also seen that the SSI modes have the most energy among the other system modes. Thus, reduction of system order even up to 2-state will preserve the SSI modes.

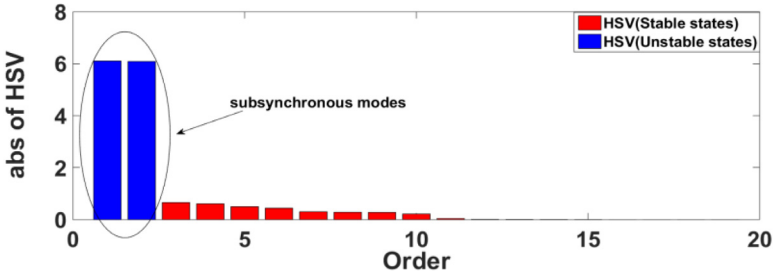

Fig. 4. Reduced order system HSVs.

The selection of the weighting factors ($\mathbf{W_1}$ and $\mathbf{W_2}$) is a common practice in the H^∞ multi-objective technique [24]. The weighting function $\mathbf{W_1}$ is a low-pass filter with a cut-off frequency of 5 Hz, and $\mathbf{W_2}$ is a high-pass filter with a cut-off frequency of 160 Hz. These frequencies are obtained to reject disturbances and noise in the behavior of the system. For instance, the objective of $\mathbf{W_2}$ is to reject noise and minimize control efforts in high-frequencies, which are resulted from the switching harmonics of the converters. These cut-off frequencies are obtained based on the time domain simulations and specifications of the under-study system.

Besides H^∞ design approach, pole placement constrain is also included in the LMI conditions of the design procedure to confine the eigenvalue of the closed-loop system in the pre-defined region. The LMI region has been chosen to determine the trade-off between the maximum damping, acceptable transient behavior and avoiding converter saturation. The controller is designed for the circumstances in which the SSI problem is the most severe (i.e. the slowest permissible wind speed). α is selected as -4. It should be mentioned that the LMIs may have no solutions. In such a case, the controller with the defined specification does not exist. On this basis, the design parameters are selected so that (i) the LMIs have solutions and (ii) the system damping performance becomes acceptable.

5. EMT simulations

The simulations have been performed using EMTP [27] with 50 μs time step and using the generic WT models in [28]. The DFIG converters are represented with average value models (AVMs).

The simulation scenarios are presented in Table 1. $\sigma(\eta,\ \beta)$ represents the Gaussian distribution in which the mean value and standard deviation are equal to η and β, respectively. In all the scenarios, a three-phase bolted fault is applied at the WF end of Line-2 and removed by the Line-2 circuit breakers. (CB1 and CB2 in Fig. 1(a)). The fault clearing times of CB1 and CB2 are 80 and 60 ms, respectively.

Table 1. Simulation scenarios.

Scenario	SSDC	Wind speed	Outage	Scenario	SSDC	Wind speed	Outage
S1	Without SSDC	σ (0.7 pu, 0.1 pu)	No outage	S5	Without SSDC	0.6 pu	No outage
S2	With SSDC	σ (0.7 pu, 0.1 pu)	No outage	S6	With SSDC	0.6 pu	No outage
S3	With SSDC	σ (0.7 pu, 0.1 pu)	34 × 4 WTs	S7	Without SSDC	0.6 pu	34 × 4 WTs
S4	With SSDC	σ (0.7 pu, 0.1 pu)	Cluster I and II	S8	With SSDC	0.6 pu	34 × 4 WTs

The scenarios S1 to S4 are also simulated using the aggregated representation of each cluster to validate the aggregated model precision. Reader may refer to [28] for calculation of the aggregated WT model parameters, and to [29] for calculation of equivalent MV collector grid parameters.

The active and reactive power outputs of WF Cluster-1 (see Fig. 1(b)) are presented Figs. 5–10. The EMT simulation results presented in Figs. 5, 9 and 10 indicate an SSI problem following the fault removal, and they are correlated with the eigenvalue analysis presented in Fig. 2(b). The severity of the SSI problem increases with the decrease in wind speed and for certain WT outage scenarios. As seen in Figs. 5–10, the proposed SSDC provides desired SSI damping while maintaining the desired DFIG transient performance. Moreover, Figs. 6–10 confirm the precision of the aggregated model based on average wind speed assumption. Although not presented here, the accuracy of the aggregated model is similar in simulation scenarios S5–S8.

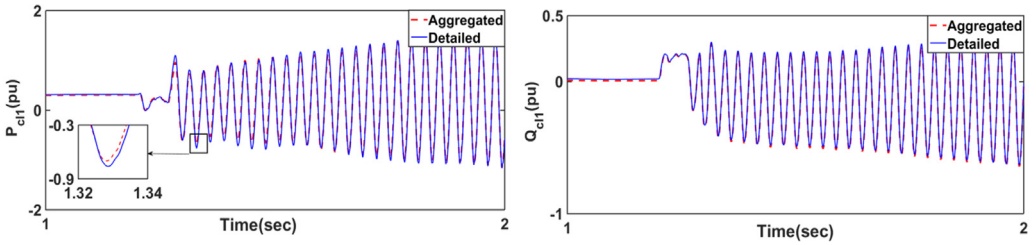

Fig. 5. WF Cluster-1 active and reactive powers (Scenario S1).

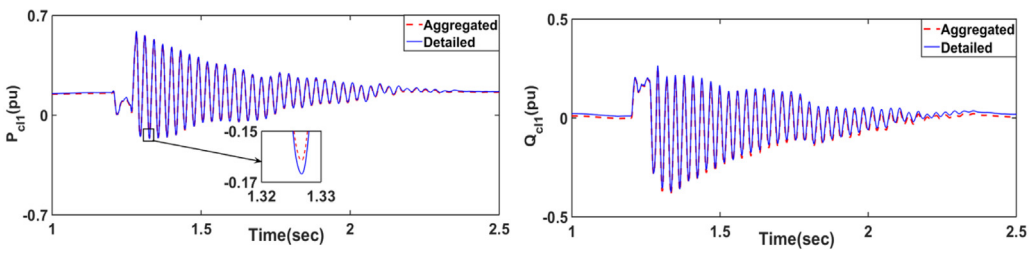

Fig. 6. WF Cluster-1 active and reactive powers (Scenario S2).

6. Conclusions

This paper used mixed-sensitivity H^{∞} control and pole placement technique to design a robust and practicable SSDC for SSI mitigation in a series compensated DFIG-based WF. The proposed controller was integrated into

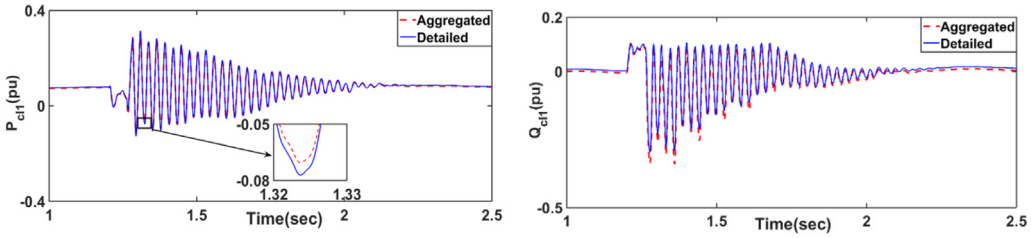

Fig. 7. WF Cluster-1 active and reactive powers (Scenario S3).

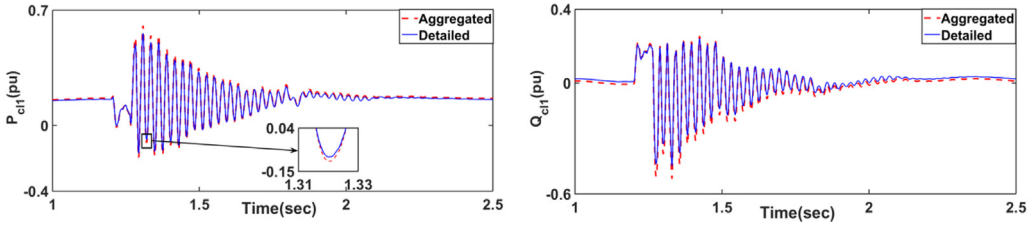

Fig. 8. WF Cluster-1 active and reactive powers (Scenario S4).

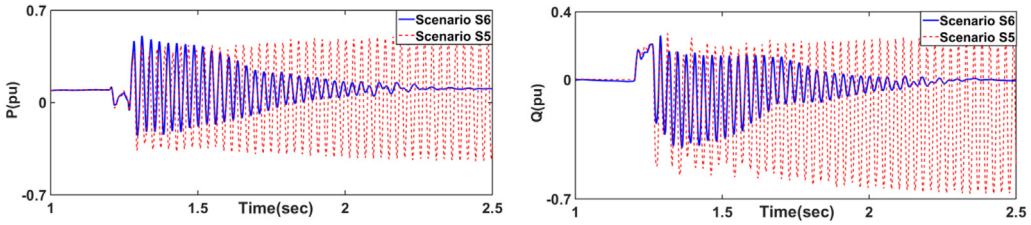

Fig. 9. WF Cluster-1 active and reactive powers (Scenarios S5 and S6).

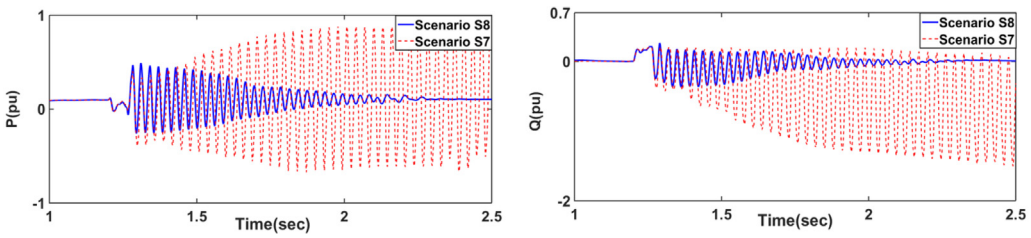

Fig. 10. WF Cluster-1 active and reactive powers (Scenarios S7 and S8).

the DFIG control system, and it receives only the RSC and GSC currents as inputs. Its implementation does not require any communication links between WTs and the WF secondary control layer. The SSDC output signals were supplemented to the RSC and GSC inner control loops. The desired FRT operation of the DFIG was achieved by limiting the SSDC output signal dynamically to avoid saturating the DFIG converters.

The simple linearized system model was used for the SSDC design. The linearization was performed for the slowest permissible wind speed to account for worst condition. However, the effectiveness of the SSDC was demonstrated through EMT simulations for various wind speed and WT outage scenarios. The simulation model of the WF was complete. All details regarding MV collector grid was represented and different wind speeds at each WT was considered. Unlike the most of the previous research in literature, the WF realistic structure and potential implementation challenges are accounted in mitigation design.

EMT simulations verified the effectiveness of the proposed SSDC. The desired SSI damping was achieved without affecting the DFIG transient responses against faults. EMT simulations also confirmed the accuracy of the aggregated model that uses the average wind speed.

Declaration of competing interest

The authors declare no conflict of interest.

Data availability

No data was used for the research described in the article.

Acknowledgments

This work was partially supported by the Hong Kong Research Grant Council for the Research Project under Grant 25223118 and partially supported by the Natural Sciences and Engineering Research Council of Canada.

References

[1] Fan L, Zhu C, Miao Z, Hu M. Modal analysis of a DFIG-based wind farm interfaced with a series compensated network. IEEE Trans Energy Convers 2011;26(4):1010–20.
[2] Cheng Y, et al. Real-world subsynchronous oscillation events in power grids with high penetrations of inverter-based resources. IEEE Trans Power Syst 2022;(2022). early access.
[3] Leon AE, Solsona JA. Sub-synchronous interaction damping control for DFIG wind turbines. IEEE Trans Power Syst 2015;30(1):419–28.
[4] Karaagac U, Faried SO, Mahseredjian J, Edris AA. Coordinated control of wind energy conversion systems for mitigating subsynchronous interaction in DFIG-based wind farms. IEEE Trans Smart Grid 2014;5(5):2440–9.
[5] Huang PH, El Moursi MS, Xiao W, Kirtley JL. Subsynchronous resonance mitigation for series-compensated DFIG-based wind farm by using two-degree-of-freedom control strategy. IEEE Trans Power Syst 2015;30(3):1442–54.
[6] Chowdhury MA, Mahmud MA, Shen W, Pota HR. Nonlinear controller design for series-compensated DFIG-based wind farms to mitigate subsynchronous control interaction. IEEE Trans Energy Convers 2017;32(2):707–19.
[7] Mohammadpour HA, Ghaderi A, Mohammadpour H, Santi E. SSR damping in wind farms using observed-state feedback control of DFIG converters. Electr Power Syst Res 2015;123:57–66.
[8] Mohammadpour HA, Santi E. Optimal adaptive sub-synchronous resonance damping controller for a series-compensated doubly-fed induction generator-based wind farm. IET Renew Power Gener 2015;9(6):669–81.
[9] Taherahmadi J, Jafarian M, Asefi MN. Using adaptive control in DFIG-based wind turbines to improve the subsynchronous oscillations of nearby synchronous generators. IET Renew Power Gener 2017;11(2):362–9.
[10] Ghafouri M, Karaagac U, Karimi H, Jensen S, Mahseredjian J, Faried SO. An LQR controller for damping of subsynchronous interaction in DFIG-based wind farms. IEEE Trans Power Syst 2017;32(6):4934–42.
[11] Ghafouri M, Karaagac U, Karimi H, Mahseredjian J. Robust subsynchronous interaction damping controller for DFIG-based wind farms. J Mod Power Syst Clean Energy 2019;7(6):1663–74.
[12] Ghafouri M, Karaagac U, Mahseredjian J, Karimi H. SSCI damping controller design for series compensated DFIG based wind parks considering implementation challenges. IEEE Trans Power Syst 2019;34(4):2644–53.
[13] Ghafouri M, Karaagac U, Kocar I, Xu Z, Farantatos E. Analysis and mitigation of the communication delay impacts on wind farm central SSI damping controller. IEEE Access 2021;9:105641-105650.
[14] Ghafouri M, Karaagac U, Ameli A, Yan J, Assi C. A cyber attack mitigation scheme for series compensated DFIG-based wind parks. IEEE Trans Smart Grid 2021;12(6):5221–32.
[15] Chaudhuri B, Pal B, Zolotas A, Jaimoukha I, Green T. Mixed-sensitivity approach to h∞ control of power system oscillations employing multiple FACTS devices. IEEE Trans Power Syst 2003;18(3):1149–56.
[16] Chaudhuri B, Pal B. Robust damping of multiple swing modes employing global stabilizing signals with a TCSC. IEEE Trans Power Syst 2004;19(1):499–506.
[17] Li Y, Sun Y, Dai X. Mu-synthesis for frequency uncertainty of the ICPT system. IEEE Trans Ind Electron 2013;60(1):291–300.
[18] Bevrani H, Feizi M, Ataee S. Robust frequency control in an islanded microgrid: Hinf and Mu synthesis approaches. IEEE Trans Smart Grid 2016;7(2):706–17.
[19] Babazadeh M, Karimi H. μ-Synthesis control for an islanded microgrid with structured uncertainties. In: 37th annual conference on IEEE industrial electronics society. Melbourne, Australia; 2011, p. 3064–9.
[20] Boukarim G, Wang S, Chow J, Taranto G, Martins. A comparison of classical, robust, and decentralized control designs for multiple power system stabilizers. IEEE Trans Power Syst 2000;15(4):1287–92.
[21] Gahinet P, Apkarian P. A linear matrix inequality approach to h control. Int J Robust Non-Linear Control 1994;4:421–8.
[22] Karaagac U, Mahseredjian J, Jensen S, Gagnon R, Fecteau M, Kocar I. Safe operation of DFIG based wind parks in series compensated systems. IEEE Trans Power Deliv 2018;33(2):709–18.
[23] Skogestadand S, Postlethwaite I. Multivariable feedback control, analysis and design. Wiley; 2005.

[24] Duan G, Yu H. LMIs in control systems: analysis, design and applications. CRC Press; 2013.
[25] Chilali M, Gahinet P, Apkarian P. Robust pole placement in LMI regions. IEEE Trans Automat Control 1999;44(12):2257–70.
[26] Gu D, Petkov P, Konstantinov M. Robust control design with MATLAB. London, UK: Springer-Verlag; 2005.
[27] Mahseredjian J, Dennetière S, Dubé L, Khodabakhchian B, Gérin-Lajoie L. On a new approach for the simulation of transients in power systems. Electr Power Syst Res 2007;77:1514–20.
[28] Karaagac U, Saad H, Peralta J, Mahseredjian J. Doubly-fed induction generator based wind park models in EMTP-RV. Research report 2015, Polytechnique Montréal; 2015.
[29] Muljadi E, et al. Equivalencing the collector system of a large wind power plant. In: IEEE PES general meeting. Montreal, Canada; 2006, p. 1–5.